

Graphene as an electronic membrane

EUN-AH KIM¹ and A. H. CASTRO NETO^{2(a)}

¹ *Stanford Institute for Theoretical Physics and Department of Physics, Stanford University - Stanford, CA 94305, USA*

² *Department of Physics, Boston University - 590 Commonwealth Avenue, Boston, MA 02215, USA*

received 24 July 2008; accepted in final form 27 October 2008

published online 10 December 2008

PACS 73.20.-r – Electron states at surfaces and interfaces

PACS 61.48.De – Structure of carbon nanotubes, boron nanotubes, and closely related graphitelike systems

PACS 81.05.Uw – Carbon, diamond, graphite

Abstract – We investigate the membrane aspect of graphene and its impact on the electronic properties. We show that rippling generates spatially varying electrochemical potential that is proportional to the square of the local curvature. This is due to the rehybridization effects and the change in the next-neighbor hopping caused by curvature. We estimate the electrochemical-potential variation associated with the rippling observed in recent scanning tunneling microscopy (STM) to be of order 30 meV. Further we show that the charge inhomogeneity in turn stabilizes ripple formation.

Copyright © EPLA, 2008

The rippling tendency [1–3] and the charge inhomogeneity [4] are both among recently revealed real-life aspects of graphene [5] that go beyond the ideal picture of relativistic Dirac fermions in pristine two-dimensional (2D) space. The observations of ripples using multiple local probes [1–3] brought the membrane aspect of graphene to the foreground. In fact, graphene is the very first example of an *electronic membrane* that is subject to local probes and to gating. This offers a new perspective for appreciating physics of membranes in addition to soft matter (especially biological systems) perspective [6]. The observations of electron-hole puddles in graphene using scanning single-electron transistor (SET) [4] offers an important clue as to what is limiting the transport properties of graphene. Clearly understanding the cause of such charge inhomogeneity is essential for the needed quality control towards device applications. Moreover, understanding the interplay between the membrane aspect and electric aspect is timely as experimentalists are beginning to exploit the membrane aspect [7,8].

In this letter, we establish the one-to-one connection between two aspects of graphene: the local curvature, which is a membrane aspect, and the local electrochemical potential, an electronic aspect. We build an effective theory based on microscopic calculations and find the corrugations to generate inhomogeneous electrochemical potential directly on the graphene membrane. Specifically,

we discuss two mechanisms for curvature to cause an electrochemical-potential variation: a) by inducing rehybridization between nearest neighbors, b) by affecting the next-to-nearest-neighbor (n.n.n.) hopping integral t' . Hence we identify corrugations as a cause of charge inhomogeneity, in addition to remote charged impurities in the substrate previously discussed in refs. [9,10]. In order to make our predictions quantitative, we calculate a map of electrochemical potential corresponding to a model solution for a ripple configuration with all model parameters extracted from a recent STM measurements [3].

Elastic free energy and local mean curvature.

– We are ultimately interested in quantitatively modeling a ripple configuration and calculating local curvature distribution. For this, we need a framework for modeling a membrane configuration. A good starting point is the parametrization-independent bending free energy describing a free, almost flat membrane in the thermodynamic limit [11]:

$$E_{bending} = \int ds_1 ds_2 \sqrt{g} \left[\gamma + \frac{1}{2} \kappa (2H)^2 + \bar{\kappa} K \right], \quad (1)$$

where (s_1, s_2) are intrinsic coordinates, g is the determinant of the metric, H and K are, respectively, the mean and the Gaussian curvature at the given point. If R_1 and R_2 are the local principle radii of curvature $H = (R_1^{-1} + R_2^{-1})/2$ and $K = (R_1 R_2)^{-1}$. In eq. (1), the tension γ , the bending rigidity κ , and the Gaussian rigidity

^(a)E-mail: neto@bu.edu

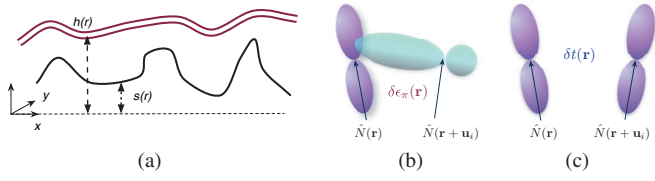


Fig. 1: Graphene as an electronic membrane. (a) The reference \mathbf{r} -plane is shown as a dashed line. The height of the curved graphene surface and the substrate surface measured from this plane, are denoted by $h(\mathbf{r})$ and $s(\mathbf{r})$, respectively. (b) The π - σ rehybridization due to the curvature which results in local electrochemical-potential variation. (c) The curvature-dependent hopping integral which depends on the overlap $\hat{N}(\mathbf{r}) \cdot \hat{N}(\mathbf{r} + \mathbf{u}_i)$ introduces a local “vector potential”.

$\bar{\kappa}$ are parameters characterizing a given membrane. $\kappa \approx 1$ eV has been measured recently in graphene electro-mechanical resonators [7] in agreement with microscopic calculations [12,13]. While γ and $\bar{\kappa}$ are not known directly from measurements, we find that the relevant length scale associated with γ can be extracted from recent STM measurements [3].

Application of eq. (1) to graphene depends on the graphene setup of interest. The crumpling possibility, which was first noted in ref. [1] comes out of studying the free energy eq. (1) in the tensionless $\gamma = 0$ limit [6]. However eq. (1) as is, only applies to membranes floating in solution, without external symmetry-breaking field to set the coordinates. When graphene is held in place either by a substrate or by a scaffold, we need to add a potential V to eq. (1). The fixation represented by the potential V breaks translational symmetry in the direction perpendicular to the device plane and also provides a natural parametrization: a Mongé representation $(x, y, h(\mathbf{r}))$ for the membrane configuration approximately parallel to the (x, y) -plane (see fig. 1). The potential $V(h, s)$ includes effects of external pressure, an attraction to the support such as Van der Waals attraction, and a repulsive force, where $s(\mathbf{r})$ is the height of the substrate. Following ref. [14], we expand $V(h, s)$ to second-order assuming the attraction is local. The resulting free energy is

$$\mathcal{F}[h] = \int d\mathbf{r} \left[\gamma + \frac{1}{2} \gamma (\nabla h)^2 + \frac{1}{2} \kappa (\nabla^2 h)^2 + \frac{1}{2} v (h - h_0 - s)^2 \right], \quad (2)$$

where $v = \partial^2 V(h_0, s) / \partial h^2$ for equilibrium configuration h_0 . Notice the term proportional to κ is the mean curvature H term of eq. (1) expressed in the chosen parametrization and we ignored the Gaussian curvature term. Since the Gaussian curvature term is a total derivative, it can be ignored for a membrane with fixed topology according to Gauss-Bonnet theorem. (This is not to mean that the value of the integral will be zero. Rather, the focus of this work is local fluctuations that do not change the global topology, for which the integral remains constant [15].)

Curvature effects on electronic structure. – The effect of the finite curvature on the band structure can be understood within the Slater-Koster prescription. There are two main effects: a) the π - σ rehybridization between nearest neighbors shifts the π -orbital energy, resulting in an effective electrochemical-potential variation; (b) the change in the nearest-neighbor hopping integral introduces effective “vector potential”. The effect (a) leads to one-to-one correspondence between mean curvature and charge inhomogeneity: the main result of this letter.

The low-energy effective Hamiltonian in the vicinity of a Dirac point $\vec{K} = (4\pi/3\sqrt{3}a, 0)$ can be written as [5]

$$H = \int d\mathbf{r} \Psi^\dagger(\mathbf{r}) \left\{ \vec{\sigma} \cdot [i v_F \nabla + \vec{\mathcal{A}}(\mathbf{r})] - \mu + \Phi(\mathbf{r}) + U(\mathbf{r}) \right\} \Psi(\mathbf{r}), \quad (3)$$

where $v_F \equiv 3ta/2$ for the bare nearest-neighbor hopping integral $t = 2.7$ eV and nearest-neighbor distance $a = 2.5$ Å, $\vec{\sigma} = (\sigma_x, \sigma_y)$ are Pauli matrices in the sublattice basis. $\vec{\mathcal{A}}(\mathbf{r})$ and $\Phi(\mathbf{r})$ are the curvature-induced “vector potential” and the electrochemical potential of our interest. $U(\mathbf{r})$ is the charged impurity potential outside the scope of this letter. (The effect of $U(\mathbf{r})$ depends on the impurity strength and the screening [9,10], which are not known from first principles.)

The curvature-induced rehybridization between nearest neighbors shifts the π level energy and contributes to $\Phi(\mathbf{r})$. The rehybridization couples the π -orbitals to the σ -bonds and antibonds, and to the $3s$ -orbitals at the higher energy ϵ_s^* (see fig. 1(b)). We calculate this shift $\delta\epsilon_\pi$ through the standard second-order perturbation theory. In the standard notation [16] these matrix elements for each of these two types of perturbation can be expressed as $\frac{1}{2}(V_{sp\sigma}^2 + V_{pp\sigma}^2)$ and $V_{s^*p\sigma}$. It is then straightforward calculate $\delta\epsilon_\pi$ (see footnote¹):

$$\delta\epsilon_\pi = \left[\frac{1}{2}(V_{sp\sigma}^2 + V_{pp\sigma}^2) \left(\frac{1}{\epsilon_\pi - \epsilon_b} + \frac{1}{\epsilon_\pi - \epsilon_a} \right) + \frac{V_{s^*p\sigma}^2}{\epsilon_\pi - \epsilon_s^*} \right]. \quad (4)$$

For graphene, the relevant energies can be found in ref. [16]: $V_{sp\sigma} = 1.43$ eV, $V_{pp\sigma} = 7.13$ eV, $\epsilon_\pi = -11.07$ eV, $\epsilon_b = -24.34$ eV, $\epsilon_a = -3.34$ eV and $V_{s^*p\sigma} / (\epsilon_\pi - \epsilon_s^*) = -1.01$ eV. This gives $\delta\epsilon_\pi = -3.23$ eV.

Another contribution to $\Phi(\mathbf{r})$ comes from mean-curvature effects on the next-to-nearest-neighbor hopping integral $t' \approx 0.1$ eV [17], which effectively generates the local electrochemical potential of $3t'$. Hence, curvature-induced variations $\delta t'$ lead to local changes in the chemical potential². Such contribution $\Phi(\mathbf{r})$ can be written as: $\Phi_{\text{mn}}(\vec{R}_i) = 6 \sum_{\vec{\delta}} \delta t'_i(\vec{\delta}) e^{-i\vec{\delta} \cdot \vec{K}}$, where $\delta t'_i = (-t'/3 + V'_{pp\sigma}/2) [(\vec{\delta} \cdot \nabla) \nabla h]^2$ with $V'_{pp\sigma} \approx +1.4$ eV [18] and $\vec{\delta}$ are the next nearest-neighbor vectors. (An idea related to this effect was discussed in ref. [19].)

¹We thank W. Harrison for pointing this out to us.

²We thank S. Kivelson for this suggestion.

The combined effect of rehybridization and next-to-nearest-neighbor hopping is

$$\Phi(\mathbf{r}) = -\alpha \frac{3a^2}{4} (\nabla^2 h)^2, \quad (5)$$

where $\alpha = -3t' + 9V'_{pp\sigma}/2 + |\delta\epsilon_\pi| \approx 9.23$ eV. Together with the elastic free energy of the membrane, eq. (2), and the effective electronic Hamiltonian, eq. (3), eq. (5) defines a coupled problem between curvature and fermion bilinears. In particular, it shows the direct connection between the local mean curvature $\nabla^2 h$ and the local electrochemical potential $\Phi(\mathbf{r})$ that couples to the charge density. The spatially varying $\Phi(\mathbf{r})$ resulting from local curvature will off-set the charge neutrality point from the average chemical potential μ_0 . More specifically, a flatter region with $|\nabla^2 h| < 1/R_c$ will be locally hole doped while a bumpier region with $|\nabla^2 h| > 1/R_c$ will be locally electron doped with a critical length scale $R_c/a = \sqrt{3\alpha/4\mu_0}$. In turn, the spatially varying charge density $n(\mathbf{r})$ enhances the rippling tendency by renormalizing the bending rigidity

$$\kappa(\mathbf{r}) = \kappa_0 - \alpha \frac{3}{4} a^2 n(\mathbf{r}). \quad (6)$$

For completeness, we express the effective “vector potential” $\vec{\mathcal{A}}$ due to the mean-curvature-driven change in the nearest-neighbor hopping integral. Misalignment of the angle θ between neighboring π -orbitals in the presence of local curvature affects the hopping integral $V_{pp\pi}(=t)$ between neighboring π -orbitals and it becomes $(V_{pp\pi} \cos^2 \theta - \frac{3}{2} V_{pp\sigma} \sin^2 \theta) \approx V_{pp\pi} - (V_{pp\pi} + \frac{3}{2} V_{pp\sigma}) \theta^2$ and $\theta^2 \sim ((\vec{u}_j \cdot \nabla) \nabla h)^2$ (see fig. 1(c)). The resulting “vector potential” is

$$\mathcal{A}_x(\mathbf{r}) + i\mathcal{A}_y(\mathbf{r}) = - \sum_j \frac{\epsilon_{\pi\pi}}{2} ((\vec{u}_j \cdot \nabla) \nabla h)^2 e^{i\vec{u}_j \cdot \vec{K}} \quad (7)$$

with $\epsilon_{\pi\pi} = V_{pp\pi}/3 + V_{pp\sigma}/2 = 2.89$ eV (See ref. [16] for the definition of parameters). Here \vec{u}_i 's are three nearest-neighbor vectors $\vec{u}_1 = a(\sqrt{3}/2, 1/2)$, $\vec{u}_2 = a(-\sqrt{3}/2, 1/2)$, $\vec{u}_3 = a(0, -1)$, and hence $\mathcal{A}_x = -\epsilon_{\pi\pi} \frac{3a^2}{8} [(\partial_x^2 h)^2 - (\partial_y^2 h)^2]$, $\mathcal{A}_y = \epsilon_{\pi\pi} \frac{3a^2}{4} [\partial_{x,y}^2 h (\partial_x^2 h + \partial_y^2 h)]$. Mechanisms for effective “gauge field” generation has been discussed earlier in refs. [20–22] and more recently (after submission of this paper) in [19,23–25]. These fictitious gauge fields [20] are known to lead to anomalies in the density of states [26] and to suppression of weak localization [21,22].

We note in passing that while the curvature can induce electron-electron interaction and electron self-energy corrections, which can be understood via standard perturbation theory starting from the bilinear coupling in eq. (3), these are effects of higher order (fourth order) in the weak long-wavelength variation of the curvature for a nearly flat membrane. Another sub-leading effect of mean curvature is through the “vector potential” $\vec{\mathcal{A}}$ [21]. Since the “field” $\nabla \times \vec{\mathcal{A}}$ reverses its direction at the other Dirac point \vec{K}' , in the presence of valley

degeneracy, the lowest-order effect on fermion properties of the curvature through $\vec{\mathcal{A}}$ is also of the fourth order in curvature [22]. In the presence of topological defects, the Gaussian curvature can have more direct consequence in introducing the effective random gauge field [15]. However, this is outside the focus of the present paper.

Ripple solutions with experimental input. – In order to estimate the curvature-induced electrochemical potential in the observed ripple configurations, we first solve for the ripple configuration $h(\mathbf{r})$ which minimizes the free energy, eq. (2), as a function of material parameters γ and κ . In principle, the coupled problem defined by eqs. (2), (3) and (5) should be solved self-consistently. However, when the thermal fluctuation of the membrane is weak, such mean-field theory treatment of the membrane allows tractable analytic progress [14]. The Euler-Lagrange equation for minimizing the free energy, eq. (2), is

$$(\kappa \nabla^4 - \gamma \nabla^2 + v) \delta h(\mathbf{r}) = v s(\mathbf{r}), \quad (8)$$

where $\delta h \equiv h(\mathbf{r}) - h_0$. Equation (8) defines two relevant length scales: $\xi_\kappa \equiv (\kappa/v)^{1/4}$ and $\xi \equiv (\kappa/\gamma)^{1/2}$. ξ_κ determines how closely the membrane follows the external potential and ξ determines the spatial extent of the curvature variation.

The relevant length scales $\xi_\kappa \equiv (\kappa/v)^{1/4}$ and $\xi \equiv (\kappa/\gamma)^{1/2}$ can be in fact estimated from the data analysis of recent experiments [2,3], while it is hard to measure the individual parameters of eq. (8). In particular, Ishigami *et al.* reported [3] the graphene height variation under ultrahigh vacuum condition to range over $\Delta h_{\max} \sim \pm 0.5$ nm around the average height of $\bar{h} \sim 0.4$ nm with a standard deviation of $\delta \bar{h} \sim 0.19$ nm. They further analyzed the height-height correlation function to find the roughness exponent to be $2H \sim 1$, which is close to that of the SiO₂ substrate. They also find the roll-over length scale (the length scale at which the correlation rolls over to a saturated behavior) to be larger (~ 32 nm) for graphene than for SiO₂ (~ 23 nm). This analysis suggests that graphene is following the substrate potential in a coarse-grained and smooth manner. We construct a model description with adjustable length scales for a graphene membrane on a random supporting potential. We then determine the length scales guided by the observations of ref. [3]. From this model we calculate the associated electrochemical-potential variation which can be compared with future measurements.

We model the graphene configuration by investigating the solution of eq. (8) for a piecewise constant potential. As a specific example, we considered a pillar of radius R , height l (*i.e.* $s(r) = l$ for $\rho \leq R$ and $s(r) = 0$ for $r > R$) and a pit of radius R and depth l' ($s(r) = -l'$ for $r \leq R$ and $s(r) = 0$ for $r > R$). We chose $l = 0.5$ nm, $l' = 9.2$ nm, $R = 1$ nm to generate a single-ripple configuration with a height variation range of $\Delta h_{\max} \sim \pm 0.5$ nm extending over a $\Delta r \sim 10$ nm radius (see fig. 2) as

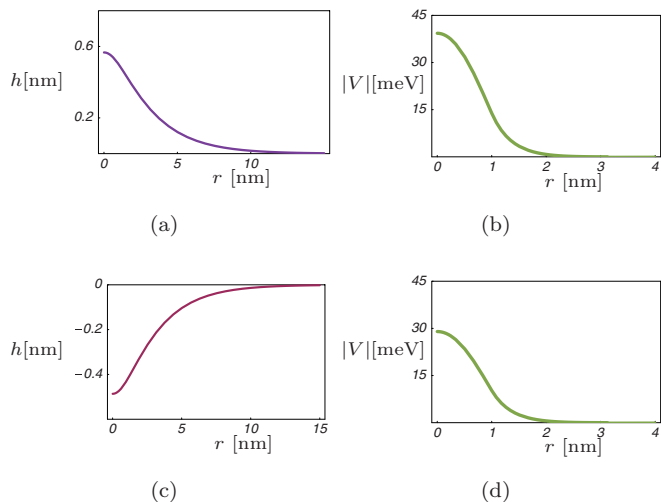


Fig. 2: Configurations for ripples due to (a), (b) a pillar of height $l = 0.5$ nm and (c), (d) a pit of depth $l' = 9.2$ nm, both cases with radius $R = 1$ nm. The membrane configurations $h(r)$ in (a) and (c) are solutions of eq. (8) for $\xi = 1.3$ nm and $\xi_\kappa = 2$ nm. The corresponding electrochemical potential $V(r)$ are shown in (b) and (d) as a function of r .

observed in refs. [1–3] for $\xi = 1.3$ nm and $\xi_\kappa = 2$ nm. The specific values of ξ and ξ_κ were determined based on the observed values of $\overline{\delta h}$, the roughness saturation scale and the extent of the ripple Δr . Figure 2 shows the configuration of a single ripple as a solution to eq. (8) for such potential and the corresponding electrochemical potential, eq. (5). The main feature is that, despite the abrupt nature of the supporting potential, the membrane shows an extended ripple configuration. Meanwhile, the electrochemical-potential variation associated with the curvature has a shorter range, determined by ξ_κ . The solution is qualitatively similar for different piecewise constant supporting potentials.

In terms of the above individual ripple solution, we model the membrane configuration as supported by randomly placed pillars. In this process, the average distance between the supporting centers is determined based on the observation of a 20 nm saturation scale for the height correlation of the SiO₂ substrate. Figure 3(a) shows such model configuration. Figure 3(b) shows the histogram of the graphene height distribution. The standard deviation for the distribution is $\overline{\delta h} = 0.22$ nm, close to the value observed in refs. [2,3], and the maximum deviation from the average height is $\Delta_{\max} h \approx \pm 0.5$ nm. This histogram shows that our model configuration captures the height distribution reported in refs. [2,3]. We show the contour plot of the height distribution in fig. 3(c) and calculated the electrochemical potential in fig. 3(d). The last two figures show that both hills and valleys of graphene correspond to regions of negative electrochemical potential.

Concluding remarks. – We investigated the interplay between the membrane aspect and the electronic

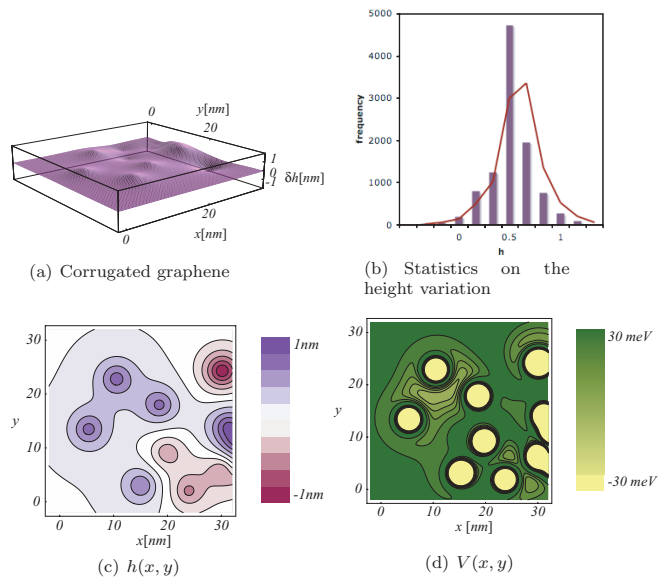


Fig. 3: A graphene sheet of size 30 nm \times 30 nm, laid on top of a random supporting potential. (a) The model graphene structure showing rippling via spatial fluctuation in the height $h(x, y)$. (b) Histogram showing the distribution of the graphene height (nm). (c) Contour plots for the local height variation $h(x, y)$ and (d) the local electrochemical-potential variation $V(x, y)$.

aspect of graphene, which is a unique example of an electronic membrane. We find one-to-one correspondence between the local mean curvature and the electrochemical potential. The spatial variation of the mean curvature in the presence of rippling, generates an electrochemical-potential variation on the graphene sheet itself through the π - σ rehybridization and locally breaks the particle-hole symmetry. Furthermore, charge inhomogeneity in turn stabilizes rippling by renormalizing the bending rigidity of the membrane. We presented a low-energy effective theory based on microscopic considerations. We further constructed a model configuration guided by experimentally observed length scales and found that the observed scale of ripple configuration generates an electrochemical-potential fluctuation of the order of ± 30 meV.

Our calculation suggests that rippling can play a significant role in driving the charge inhomogeneity, given that this chemical-potential variation is occurring directly on the graphene sheet itself. Through our simple modeling, we demonstrated how to construct a model configuration based on experimentally observable quantities. Our effective theory can be used for more detailed modeling based on detailed understanding of the supporting potential for the characterization and design of graphene-based electronic elements. We predict that a better control over irregular corrugations will improve the transport properties of graphene greatly. At present, the technology for stabilizing perfectly flat graphene is not available. One possibility is to epitaxially grow monolayer graphene in a controlled manner. While the current growth technique

only yields a few layer of graphene with the bottom layer forming the dominant channel for transport [27], likely the status will improve in a near future.

After submission of this paper, there have been more theoretical studies on the effect of rippling focusing on the effective gauge field aspect [19,23–25].

We thank M. FREEDMAN, A. GEIM, F. GUINEA, W. HARRISON, H. LIANG, M. KATSNELSON, P. KIM, S. A. KIVELSON, J. L. DOS SANTOS, R. SHANKAR, S.-W. TSAI and A. YACOBY for many illuminating discussions. We thank KITP Santa Barbara (NSF Grant PHY99-07949) for its hospitality during the completion of this work. AHCN was supported through NSF grant DMR-0343790.

REFERENCES

- [1] MEYER J. C. *et al.*, *Nature*, **446** (2007) 60.
- [2] STOLYAROVA E. *et al.*, *Proc. Natl. Acad. Sci. U.S.A.*, **104** (2007) 9209.
- [3] ISHIGAMI M. *et al.*, *Nano Lett.*, **7** (2007) 1643.
- [4] MARTIN J. *et al.*, *Nat. Phys.*, **4** (2008) 144.
- [5] See GEIM A. and NOVOSELOV K. S., *Nat. Mater.*, **6** (2007) 183; CASTRO NETO A. H. *et al.*, to be published in *Rev. Mod. Phys.*, arXiv:0709.1163, and references therein.
- [6] NELSON D., PIRAN D. R. and WEINBERG S., *Statistical Mechanics of Membranes and Surfaces* (World Scientific, Singapore) 2004.
- [7] BUNCH J. *et al.*, *Science*, **315** (2007) 490.
- [8] BUNCH J. *et al.*, *Nano Lett.*, **8** (2008) 2458.
- [9] HWANG E. H., ADAM S. and DAS SARMA S., *Phys. Rev. Lett.*, **98** (2007) 186806.
- [10] NOMURA K. and MACDONALD A. H., *Phys. Rev. Lett.*, **98** (2007) 076602.
- [11] HELFRICH W. A., *Naturforsch. C*, **28** (1973) 693.
- [12] LENOSKY T. *et al.*, *Nature*, **355** (1992) 333.
- [13] TU Z.-C. and OU-YANG Z.-C., *Phys. Rev. B*, **65** (2002) 233407.
- [14] SWAIN P. S. and ANDELMAN D., *Langmuir*, **15** (1999) 8902.
- [15] CORTIJO A. and VOZMEDIANO M. A. H., *Nucl. Phys. B*, **763** (2007) 293.
- [16] HARRISON W., *Elementary Electronic Structure* (World Scientific, Singapore) 2004.
- [17] REICH S. *et al.*, *Phys. Rev. B*, **66** (2002) 035412.
- [18] TANG M. S. *et al.*, *Phys. Rev. B*, **53** (1996) 979.
- [19] HUERTAS-HERNANDO D., GUINEA F. and BRATAAS A., *Phys. Rev. B*, **74** (2006) 155426.
- [20] KANE C. L. and MELE E. J., *Phys. Rev. Lett.*, **78** (1997) 1932.
- [21] MOROZOV S. V. *et al.*, *Phys. Rev. Lett.*, **97** (2006) 016801.
- [22] MORPURGO A. F. and GUINEA F., *Phys. Rev. Lett.*, **97** (2006) 196804.
- [23] GUINEA F., HOROVITZ B. and LE DOUSSAL P., *Phys. Rev. B*, **77** (2008) 205421.
- [24] THOMPSON-FLAGG R. C., MOURA M. J. B. and MARDER M., arXiv:0807.2938.
- [25] VAZQUEZ DE PARGA A. L. *et al.*, *Phys. Rev. Lett.*, **100** (2008) 056807.
- [26] LUDWIG A. W. W. *et al.*, *Phys. Rev. B*, **50** (1994) 7526.
- [27] BERGER C. *et al.*, *Science*, **312** (2006) 1191.